Compendium of M.Sc. Publications on Assessment of Effective Properties of Multi-phase Materials

David Uribe

EAFIT UNIVERSITY
COLLEGE OF ENGINEERING
MASTER PROGRAM IN ENGINEERING
MEDELLIN, COLOMBIA
MAY 2013

MASTER PUBLICATION

Compendium of M.Sc. Publications on Assessment of Effective Properties of Multi-phase Materials

MASTER STUDENT

David Uribe

ADVISORS

Prof. Dr. Eng. Holger Steeb

Prof. Dr. Eng. Oscar Ruiz

Submitted in partial fulfillment of the requirements for the degree of Master of Engineering in the College of Engineering of the EAFIT University

EAFIT UNIVERSITY
COLLEGE OF ENGINEERING
MASTER PROGRAM IN ENGINEERING
MEDELLIN, COLOMBIA
MAY 2013

To my parents, my friends and mentors.

Acknowledgements

To my parents Gladys and Eugenio, for the sustained love, patience, support and endurance with which they have accompanied me along my endeavors in life. I hope that life will keep us together for many, many years.

I want to express my upmost gratitude to my advisor Prof. Dr. Eng. Oscar Ruiz for all the academic and material support and always reliable recommendations that made this moment possible. His encouragement does not limit itself to academics, but reaches other aspects of my life. I also owe deep gratitude to Prof. Dr. Eng. Holger Steeb for academic, material and human support during my permanence in Ruhr Universitaet Bochum (RUB). I thank Prof. Dr. Eng. Erik H. Saenger and his team in ETH Zuerich for providing us with a great code and very interesting insights in geophysics.

I am very thankful to Dr. Eng. Ralf Jaenicke for his ever-present and solid help and to all the members of the Chair Continuous Mechanics in RUB. I am indebted to Juan J. Londono, Daniel Burgos and Sebastian Luna for compiling this LaTEX document. I owe gratitude for the very effective team-work that we materialize with Maria Camila Osorno in the area of Computational Mechanics. I thank the members of the CAD/CAM/CAE Laboratory in Universidad EAFIT since 2006 (Sebastian Durango, John Congote, Ricardo Serrano, David Restrepo, Jorge Correa) for their comradeship, help and loyalty.

I also will like to acknowledge the financial support for this research from the Colombian Administrative Department of Sciences, Technology and Innovation (COLCIENCIAS), the CAD CAM CAE Laboratory at Universidad EAFIT, and Ruhr-Universitaet Bochum.

Introduction

Multi-phase materials exhibit mechanical advantages such as high specific strength, low specific density, chemical resistance. These materials are natural occurring as well as designed in laboratories to function on very well defined tasks. One of the challenges that faces the use of these materials is to characterize its effective properties, i.e. the response of the material to different stimuli at a given length scale. This thesis focuses on the study of multi-phase materials at the microscopic level to find effective material properties at the macroscopic level. The bridge between the microscopic and macroscopic length scales has been of great interest for new numerical methods that estimate the effective properties. In the literature three main methods have been established to find these properties:

(1) The first approach to find such properties is to simulate the material at a microscopic level. This approach can be sometimes unpractical, since only a very small domain of the material can be simulated, and some characteristics of the material can be neglected.
(2) A second approach is to find the effective properties of the material with laboratory experiments, and then use this set of found properties to simulate the material with homogeneous properties. This approach has also shortcomings, since it is known that important properties of the materials can only be measured with microscopic experiments.
(3) The third option found in the literature is to use a combination of the first and second approach, namely the FE^2 method.

An example of the second approach to find effective material properties is the measurement of wave attenuation and phase velocities in two-phase materials. The study of wave propagation in two-phase materials has been established since the 50's by Biot. The study of this phenomenon can be used in scientific branches ranging from medicine to geophysics. These type of materials exhibit a wide range of practical uses such as acoustic isolation (mechanical waves at certain frequencies won't propagate in the medium), gas and fluid sequestration (due to the pore and skeleton geometry some fluids do not flow through the medium), lightweight-high resistance materials among other examples. The study of wave propagation in this materials has proven to be a useful tool to find effective parameters such as tortuosity, permeability and porosity.

The outline of this thesis is: In chapter 1 a method to bridge the microscale and macroscale using an homogenization technique based on minimal loading conditions is explained. This technique can be applied to the FE^2. On chapter 2 and 3 the use of the finite difference method is explained in the context of wave propagation simulations on the microscale. In chaper 4 the finite difference method is used to solve Stokes' equation in a fluid saturated porous material. Using a volume average

technique it is possible to calculate the permeability of the porous material and the result from the volume average technique is compared to Darcy's law. Finally in chapter 5 experimental results are compared with numerical results of the wave propagation phenomenon in fluid saturated media. It was possible to determine with great accuracy the tortuosity of an aluminum foam.

Contents

List of Figures

CHAPTER 1

Relaxed Loading Conditions for Higher Order Homogenisation Approaches

This research proposes a numerical method to estimated effective material parameters of heterogeneous nature. It introduces a new set of boundary conditions on microscale simulations that simplify the use of the FE^2 method. This paper was published in the Special Issue: 82nd Annual Meeting of the International Association of Applied Mathematics and Mechanics (GAMM), Graz 2011; Editors: G. Brenn, G.A. Holzapfel, M. Schanz and O. Steinbach. Publisher: WILEY-VCH Verlag

- Ralf Jaenicke[2]
- David Uribe[1,2]
- Oscar E. Ruiz[1]
- Holger Steeb[2]

[1] CAD CAM CAE laboratory, Universidad EAFIT
Carrera 49 No 7 Sur - 50, Medellin, Colombia
[2] Mechanics – Continuum Mechanics, Ruhr-University
Bochum, Germany

Abstract. The present paper deals with the formulation of minimal loading conditions for the application of numerical homogenisation techniques, namely the FE^2 methodology. Based on the set of volume averaging rules connecting the heterogeneous micro and the homogeneous macro scale, the minimal constraints on the deformation of a micro volume are derived for a classical Cauchy continuum as well as for a micromorphic continuum theory. For both cases, numerical studies are included highlighting the main aspects of the proposed procedure within the context of small deformations.

1. Introduction

Heterogeneous materials are well known for their peculiar effective material properties which are driven by the underlying micro topology. Under quasi-static conditions, e. g. boundary layers leading to size effects are to be observed [1, 2]. By contrast, a highly dispersive overall material behaviour of the compound can be found under high frequency loadings (sonic/ultrasonic) accounting for higher order wave modes due to micro structural degrees of freedom [3, 4].

In the following sections we will apply a mean-field-based homogenisation approach in order to describe the material properties of such materials on an effective scale. For this purpose, the heterogeneous medium on the micro scale has to be replaced by a homogeneous medium on the macro scale. The physical quantities of the macro scale will be interpreted in terms of volume averages of their microscopic counterparts. To this end, appropriate averaging rules have to be formulated defining a Dirichlet boundary value problem (BVP) on a micro volume which is considered to be representative for the entire micro structure. Transferring the microscopic stress response back to the macroscopic level, the overall constitutive relations can be replaced by a two-level simulation also stated as the FE^2 technique [5, 6] in the sequel.

Whilst the micro structure itself can be captured by a standard Cauchy continuum theory, different choices for the substitute medium are possible. Depending on the micro geometrical effects which are to be represented on the macro level different substitute media have to be considered. If the characteristic length scale of the micro structure is much smaller than the overall length scale (scale separation), a Cauchy substitute medium is sufficient to predict first order effects such as material or structural anisotropy [7]. However, higher order approaches are required if the characteristic length scales become comparable. Typical representatives of this class are e. g. Mindlin's second gradient theory [8] or the micromorphic continuum theory proposed by Eringen [9].

In the sequel, the present contribution focuses on two cases. On the one hand, the Cauchy substitute medium will be considered. On the other hand the micromorphic continuum theory will be applied on the macro scale. For both, the formulation of microscopic BVP will be discussed, where usually polynomial Dirichlet boundary conditions are taken into account. By contrast, we propose the concept of the so-called *minimal boundary or loading conditions* [10], where the loading conditions are not prescribed explicitly as a Dirichlet BVP but in an integral sense constrained by the averaging rules.

All numerical examples are limited to 2D and to the range of small deformations in the context of quasi-static deformations. Linear elasticity is assumed. The discussion which micro volume size is necessary to end up with a representative volume element is omitted.

2. First order homogenisation

Let us start with the substitution of a heterogeneous Cauchy medium by an effective homogeneous Cauchy medium. Moreover, let us assume an arbitrary shaped 2D micro volume of the size $V_m = l^2$. The micro volume is nested to a corresponding macroscopic material point via its volume centroid. Any position $\Delta\mathbf{x}$ inside the micro volume is expressed relative to the volume centroid. Taking into account the definition of the volume averaging procedure $\langle\bullet\rangle = 1/V_m \int(\bullet)\,\mathrm{d}v$, the averaging rules for the kinematic quantities read

$$\langle\Delta\mathbf{u}\rangle = \mathbf{0}, \quad \operatorname{grad}{}^{\mathrm{sym}}_{M}\mathbf{u}_M = \langle\operatorname{grad}{}^{\mathrm{sym}}_{m}\Delta\mathbf{u}\rangle = \frac{1}{V_m}\int\limits_{\partial V_m}(\Delta\mathbf{u}\otimes\mathbf{n})^{\mathrm{sym}}\,\mathrm{d}a, \tag{1}$$

cf. [5, 6], where the subscript indices m and M refer to the micro and the macro scale, respectively and $\mathbf{n}$ refers to the outer normal vector on the boundary ∂V_m of the micro volume. From the physical point of view, eq. $(1)_1$ constrains the micro volume in a

way that rigid body translation are omitted, whereas eq. $(1)_2$ states that the overall symmetric strain has to be equal to the volume average of the local strain or its boundary contribution, respectively. Usually, the kinematic averaging rules are evaluated applying a local Dirichlet BVP of the form

$$\Delta\mathbf{u} \;=\; \mathrm{grad}\,\overset{\mathrm{sym}}{_M}\mathbf{u}_M \cdot \Delta\mathbf{x} + \Delta\tilde{\mathbf{u}}. \tag{2}$$

For the additional fluctuation field $\Delta\tilde{\mathbf{u}}$, several cases can be considered:

a) $\Delta\tilde{\mathbf{u}} = \mathbf{0} \,\forall\, \Delta\mathbf{x} \in \partial V_m$. This special case represents the upper limit for the stress response of the micro volume and is commonly called Voigt limit. In general, the purely linear polynomial results in overestimated effective moduli due to clamping mechanisms at the boundary of the micro volume.
b) The fluctuation is considered to be periodic at homologous points of the micro volume surface whereas the surface traction vectors are anti-periodic. The periodic fluctuations allow the micro volume to overcome the clamping boundary conditions and to reduce the overestimated stress response of the micro volume. However, this special case requires geometrically periodic micro volumina which can not be guaranteed in general.

However there is no need to introduce polynomial loading conditions on the boundary of the micro volume. In order to circumvent the above limitations of the polynomial conditions we apply in the sequel the concept of *minimal loading conditions*, initially proposed in [10]. For this purpose, we consider eqs. (1) as integral constraints which control the deformation state of the micro volume without any further periodicity requirements. From the numerical point of view, these integral constraints can be easily implemented in a Finite Element code e. g. using a penalty formulation.

In order to circumvent too soft material response, we introduce an additional compatibility constraint. The need to do so can be easily motivated regarding Fig. 1.1 a), where a shear deformation mode is applied on an unit cell of a stiff grid structure (blue) embedded in a matrix (green, factor 0.0001 softer). The deformation only takes place in the soft phase, which obviously contradicts the real deformation behaviour of a periodic grid structure. However this effect can be corrected if one introduces the additional constraint that each phase has to contribute to the overall deformation according to its fraction of the boundary ∂V_m. The resulting deformation state is depicted in Fig. 1.1 b), c) and d) where the factor f decreases from 1 to 0.0001. For this special case, the result of the minimal loading conditions equals this one achieved applying periodic boundary conditions.

In the following, we want to study the proposed minimal loading condition concept with additional compatibility constraints for an exemplary microstructure consisting of a soft matrix filled with stiff particles. The resulting deformation states under tensile and shear conditions are depicted in Figs. 1.2 and 1.3 in comparison to these ones of the Voigt (linear displacements, upper bound) and the Reuss limits (constant tractions, lower bound). In Fig. 1.4, the normalised strain energy of the three independent deformation modes for micro volumina with different sizes is given in relation to the upper and the lower bound.

As expected the application of the minimal constraints allow the microstructure to relax significantly compared to the Voigt limit. The observed strain energies are even closer to the Reuss than to the Voigt limit. However, this effect could be a consequence of the very special choice of the microstructure with stochastically distributed stiff particles. For more precise conclusions, a series of comparable structures should be explored which remains a task for future work.

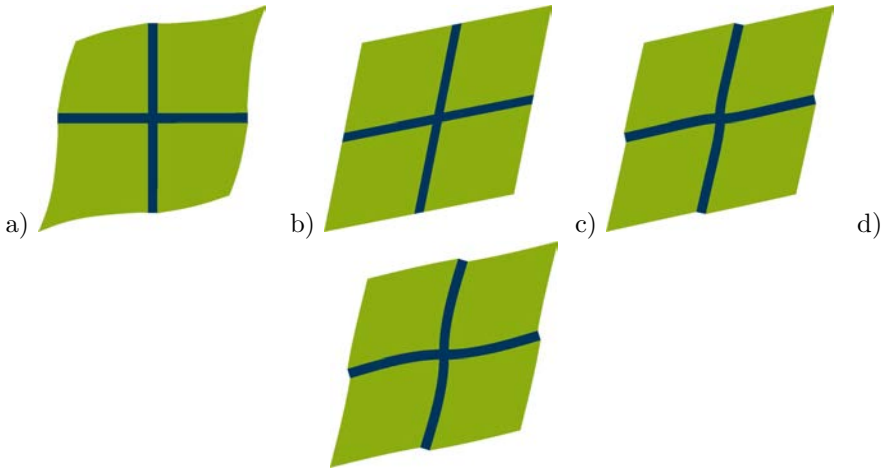

FIGURE 1.1. Shear mode $1/2\,(u_{M1,2} + u_{M2,1})$ applied on an unit cell of a stiff grid structure (blue) in a matrix (green) which is factor f softer, a) $f = 0.0001$, no additional compatibility constraint, b) $f = 1$, c) $f = 0.01$, d) $f = 0.0001$

FIGURE 1.2. Stretch mode $u_{M1,1}$ of a micro volume ($l = 4\,\mathrm{mm}$) consisting of stiff particles (blue) in a matrix (green) which is factor $f = 0.1$ softer, a) Voigt limit (linear displacements), b) minimal boundary conditions and c) Reuss limit (constant tractions).

3. Second order homogenisation

In the upcoming section we extend the concept of minimal loading conditions to a second order homogenisation scheme. For this reason, the kinematics of the substitute medium is enriched by additional degrees of freedom accounting for microscopic deformation mechanisms. Moreover, the second order extensions involve an internal length scale in an inherent way. In literature one can find basically two different approaches. The first one goes back to the seminal work of Mindlin [8] and introduces higher gradients of the overall displacement field as additional and independent degrees of freedom. The application of the second gradient continuum as a substitute medium for heterogeneous micro structures has been discussed in literature, e. g. [11, 12]. The second extension bases on the micromorphic continuum theory initially proposed by Eringen [9]. In contrast to the second gradient continuum, the so-called affine micro deformation tensor and its gradient, respectively, are introduced as independent degrees of freedom in addition to the usual displacement field. However, the micromorphic approach reduces to the second gradient

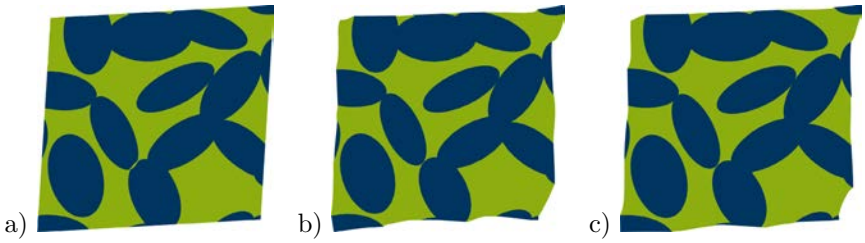

FIGURE 1.3. Symmetric shear mode $1/2\,(u_{M1,2}+u_{M2,1})$ of a micro volume ($l = 4\,\mathrm{mm}$) consisting of stiff particles (blue) in a matrix (green) which is factor $f = 0.1$ softer, a) Voigt limit (linear displacements), b) minimal boundary conditions and c) Reuss limit (constant tractions).

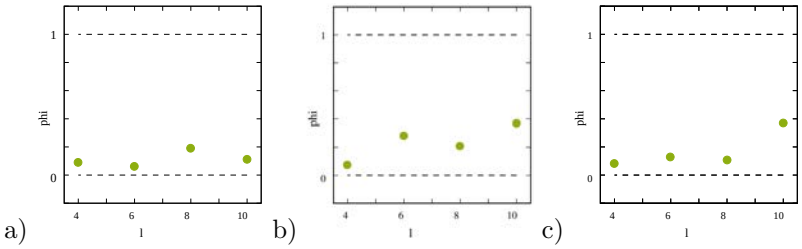

FIGURE 1.4. Strain energy observed for different micro volumina sizes l^2 activated by the deformation modes a) $u_{M1,1}$, b) $1/2\,(u_{M1,2}+u_{M2,1})$ and c) $u_{M2,2}$. The strain energy is normalised with respect to the Voigt ($\phi = 1$) and the Reuss limit ($\phi = 0$) representing homogeneous strain (linear displacements) or constant traction boundary conditions, respectively.

concept, if the micro deformation is considered to equal the first displacement gradient. In the sequel, only homogenisation rules for the micromorphic substitute medium will be discussed, which have been initially proposed by Forest et al. [13, 14, 15, 16, 17]. The kinematic averaging rules for a quadratic unit cell of the size $V_m = l^2$ read

$$\langle \Delta\mathbf{u} \rangle = \mathbf{0},\ \mathrm{grad}_M \mathbf{u}_M = \langle \mathrm{grad}_m \Delta\mathbf{u} \rangle = \frac{1}{V_m} \int\limits_{\partial V_m} \Delta\mathbf{u} \otimes \mathbf{n}\, \mathrm{d}a, \tag{3}$$

$$\bar{\boldsymbol{\chi}}_M - \mathbf{I} = \frac{12}{l^2}\, \langle \Delta\mathbf{u} \otimes \Delta\mathbf{x} \rangle\,, \tag{4}$$

$$\mathbf{K}^3_M = \mathrm{grad}_M \bar{\boldsymbol{\chi}}_M = \frac{12}{l^2}\, \langle \mathrm{grad}_m (\Delta\mathbf{u} \otimes \Delta\mathbf{x}) \rangle = \frac{1}{V_m} \int\limits_{\partial V_m} \Delta\mathbf{u} \otimes \Delta\mathbf{x} \otimes \mathbf{n}\, \mathrm{d}a. \tag{5}$$

The crucial point of these relation can be observed regarding eq. (4), which can not be transformed into a surface integral. By consequence it is not possible to prescribe Dirichlet type conditions on the boundary ∂V_m [14]. In literature, several approaches are to be found [13, 15] dealing with a cubic polynomial for the microscopic displacement field. However, the displacement field has to be prescribed on the entire micro volume V_m. No reduction to its boundary ∂V_m is known, besides some special cases of regular grid

structures [16, 17]. Thus, we propose to apply the concept of minimal loading condition for the second order homogenisation scheme. Besides the lacking periodic requirements this concept bears the advantage of circumventing a priori the formulation of any polynomial conditions. Eqs. (3–5) represent the minimal set of integral constraints enforcing the micro volume to undergo deformation modes driven by the overall kinematic quantities. Again, this concept can be easily implemented from a numerical point of view making use of a penalty formulation for instance.

In Fig. 1.5, several exemplary micromorphic deformation modes are given. The found results (Cosserat micro rotations of regular grid structures and bending mode of orthotropic unit cell) have been observed in literature [14, 16] applying polynomial loading conditions.

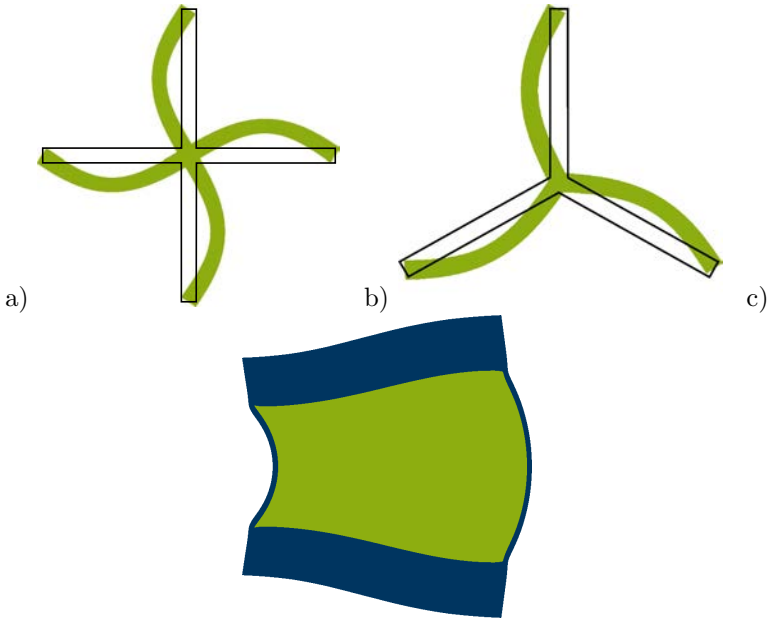

FIGURE 1.5. The Cosserat type micro rotation $\bar{\varphi}_{M3} = \bar{\chi}_{M21} = -\bar{\chi}_{M12} = 1$, applied on the unit cells of a) the squared grid and b) the honeycomb structure. The Cosserat bending mode $\bar{\varphi}_{M3,2} = -K_{M122} = 2\,K_{M122} = 2\,K_{M121} = 1/\text{mm}$, applied on the orthotropic unit cell c).

4. Conclusions

Finally, let us recall the basic findings of the present contribution addressing numerical homogenisation schemes. A general concept for the formulation of minimal loading conditions in terms of integral constraints on the micro volume has been introduced. In the case of first order homogenisation this procedure bears the advantage that no periodicity requirements exist on the geometry of the micro volume. In principle, even the shape of the micro volume can be chosen arbitrary and does not have to be necessarily quadratic. Comparing the strain energy stored during unit deformations of heterogeneous

micro volumina, it has been found the minimal loading conditions, enriched with an additional compatibility constraint, to result in significantly softer material responses than the Voigt limit representing the upper bound on the homogenised strain energy.

In the very last section, the concept of minimal loading conditions has been extended to the second order homogenisation technique for micromorphic media substituting a micro-heterogeneous Cauchy medium. Due to the extensions of the volume averaging concept it is no longer possible to formulate Dirichlet conditions on the boundary of the micro volume besides some special cases. For this reason, the averaging rules themselves have been used again as the minimal loading conditions for the micro volume. In comparison to the deformation behaviour of different structures, the resulting deformation modes can be validated qualitatively against examples given in literature.

In the future, further efforts have to be made in order to gain a deeper understanding of the proposed concept. Quantitative validations are planned. Finally, we intend to generalise the concept to 3D problems dealing with micro volumina resulting from CT scans of real micro structures.

Bibliography

[1] Stefan Diebels and Holger Steeb. The size effect in foams and its theoretical and numerical investigation. *Proceedings of the Royal Society of London. Series A: Mathematical, Physical and Engineering Sciences*, 458(2028):2869–2883, 2002.

[2] C. Tekoglu and P.R. Onck. Size effects in the mechanical behavior of cellular materials. *Journal of Materials Science*, 40(22):5911–5917, 2005.

[3] A. Askar and A.S. Cakmak. A structural model of a micropolar continuum. *International Journal of Engineering Science*, 6(10):583 – 589, 1968.

[4] A. Srikantha Phani, J. Woodhouse, and N. A. Fleck. Wave propagation in two-dimensional periodic lattices. *The Journal of the Acoustical Society of America*, 119(4):1995–2005, 2006.

[5] Frdric Feyel and Jean-Louis Chaboche. {FE2} multiscale approach for modelling the elastoviscoplastic behaviour of long fibre sic/ti composite materials. *Computer Methods in Applied Mechanics and Engineering*, 183(34):309 – 330, 2000.

[6] C. Miehe and A. Koch. Computational micro-to-macro transitions of discretized microstructures undergoing small strains. *Archive of Applied Mechanics*, 72(4-5):300–317, 2002.

[7] H.-G. Sehlhorst, R. Jnicke, A. Dster, E. Rank, H. Steeb, and S. Diebels. Numerical investigations of foam-like materials by nested high-order finite element methods. *Computational Mechanics*, 45(1):45–59, 2009.

[8] R.D. Mindlin. Micro-structure in linear elasticity. *Archive for Rational Mechanics and Analysis*, 16(1):51–78, 1964.

[9] A.Cemal Eringen. Simple microfluids. *International Journal of Engineering Science*, 2(2):205 – 217, 1964.

[10] Sinisa Dj. Mesarovic and Jagan Padbidri. Minimal kinematic boundary conditions for simulations of disordered microstructures. *Philosophical Magazine*, 85(1):65–78, 2005.

[11] ukasz Kaczmarczyk, Chris J. Pearce, and Nenad Biani. Scale transition and enforcement of rve boundary conditions in second-order computational homogenization. *International Journal for Numerical Methods in Engineering*, 74(3):506–522, 2008.

[12] V. Kouznetsova, M. G. D. Geers, and W. A. M. Brekelmans. Multi-scale constitutive modelling of heterogeneous materials with a gradient-enhanced computational homogenization scheme. *International Journal for Numerical Methods in Engineering*, 54(8):1235–1260, 2002.

[13] S. Forest and K. Sab. Cosserat overall modeling of heterogeneous materials. *Mechanics Research Communications*, 25(4):449 – 454, 1998.

[14] S. Forest and D.K. Trinh. Generalized continua and non-homogeneous boundary conditions in homogenisation methods. *ZAMM - Journal of Applied Mathematics and Mechanics / Zeitschrift fr Angewandte Mathematik und Mechanik*, 91(2):90–109, 2011.

[15] Ralf Jnicke, Stefan Diebels, Hans-Georg Sehlhorst, and Alexander Dster. Two-scale modelling of micromorphic continua. *Continuum Mechanics and Thermodynamics*, 21(4):297–315, 2009.

[16] Ralf Jnicke. *Micromorphic media : interpretation by homogenisation*. PhD thesis, Saarlndische Universitts- und Landesbibliothek, Postfach 151141, 66041 Saarbrcken, 2010.

[17] Ralf Jnicke and Holger Steeb. Wave propagation in periodic microstructures by homogenisation of extended continua. *Computational Materials Science*, 52(1):209 – 211, 2012. ¡ce:title¿Proceedings of the 20th International Workshop on Computational Mechanics of Materials - {IWCMM} 20¡/ce:title¿.

CHAPTER 2

Microscale Investigations of Highfrequency Wave Propagation Through Highly Porous Media

It was possible to establish from this research, that the High-Frequency limit of Biot's theory is possible to be simulated using a finite difference code. From these simulations it is possible to calculate the tortuosity of a porous material. This paper was published in the Special Issue: 83rd Annual Meeting of the International Association of Applied Mathematics and Mechanics (GAMM), Darmstadt 2012; Editors: H.-D. Alber, N. Kraynyukova and C. Tropea. Publisher: WILEY-VCH Verlag

- David Uribe[1,3]
- Erik Saenger[2]
- Ralf Jaenicke [1]
- Holger Steeb[1]
- Oscar E. Ruiz[3]

[1] Institute of Mechanics, Ruhr-University Bochum, Germany
University Street 150, 44801 Bochum, Alemania
[2] Geological Institute, ETH Zuerich, Switzerland
Sonneggstrasse 5, 8092 Zuerich, Switzerland
[3] Laboratorio de CAD/CAM/CAE, Universidad EAFIT, Medellin, Colombia
Carrera 49 No 7 Sur - 50, Medellín, Colombia

Abstract. Wave propagation in highly porous materials has a well established theoretical background. Still there are parameters which require complex laboratory experimentation in order to find numerical values. This paper presents an effective method to calculate the tortuosity of aluminum foam using numerical simulations. The work flow begins with the acquisition of the foam geometry by means of a micro-CT scanner and further image segmentation and analysis. The elastodynamic wave propagation equation is solved using a velocity-stress rotated staggered finite-difference technique. The effective wave velocities are calculated and using the fluid and, aluminum effective properties, the tortuosity is determined.

1. Introduction

The use of high resolution tomographic imaging has proven to be an adequate method to find effective material properties of complex structures [1]. Modern image analysis algorithms together with large-scale computations has brought the possibility to bring together different length scales to accurately describe material behavior. The sample is an open-cell foam with a porosity of 0.93. At the micro scale, the foam consists of struts that are joint rigidly at their ends. The struts' bulk material parameters (Young's modulus, Poisson's ratio and density) are known from quasi-static experiments. First, a description of the workflow from the image adquisition to the virtual experimental setup is explained. Afterwards some numeric results are presented and compared with physical experiment data.

2. Methodology

2.1. Image analysis. The Aluminium foam is digitized using a Computer Tomographic scanner. The resolution of the voxels is 60 μm. Using image segmentation and surface reconstruction algorithms it was possible to gather valuable geometric information, similar to Jang [2]. From the segmented data, a regular 3-D grid is constructed that closely resembles the physical geometry. The size of the grid is 400 x 400 x 400 points.

An important use of the gathered geometric information is determining the limit in which the highfrequency range from Biot's theory begins. From Steeb [3], the viscous skin depth can be calculated using equation 6. In this equation η^{fR} is the pore fluid viscocity, ρ^{fR} is the effective pore fluid density and f the frequency. If the pore radius is larger than the viscous skin depthd, then the effective coupling mechanism between the fluid and the solid phases is only inertia driven. This fact will become important in section 2.2.

$$d = \sqrt{\frac{2\eta^{fR}}{2\pi f \rho^{fR}}} \tag{6}$$

$$f_{crit} = \frac{\eta^{fR}}{\pi r^2 \rho^{fR}} \tag{7}$$

2.2. Simulation of a pressure wave propagating in a water saturated aluminium foam sample. The numerical experiments are solved with a parallelized algorithm. The elastodynamic wave equation is discretized using a rotated-staggered-grid finite-difference scheme developed by Saenger[4]. The foam sample is virtually immersed in the center of a water tank of size 400 x 400 x 804 gridpoints. A plane pressure wave is created at one end of the tank parallel to the z-direction. All the walls of the tank orthogonal to the z-direction have periodic boundary conditions. In our simulation we use is a Ricker wavelet, with a central frequency of 1KHz. It can be proven that this

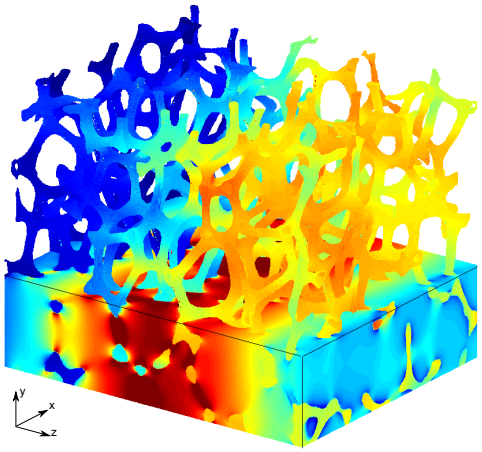

FIGURE 2.1. Aluminium foam with part of the water removed in order to see the structure. Coloring depending on pointwise velocity values.

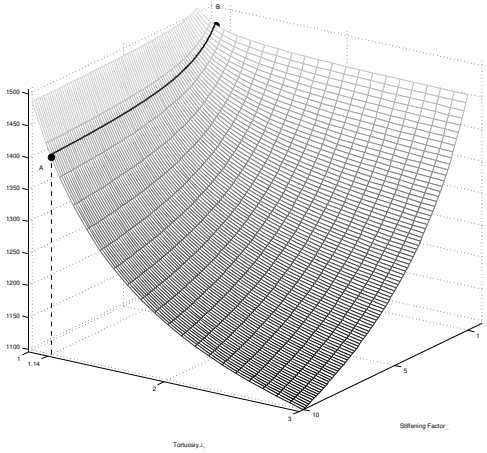

FIGURE 2.2. Analytical solution of the high-frequency limit in Biot's equation using a varying stiffening factor.

frequency is larger than the critical frequency predicted by Biot (eq. 7) and therefore lies in the high-frequency range.

In order to measure the pressure wave velocities, virtual receivers are placed right before the aluminium foam and right afterwards. These measurements are compared with a reference simulation (the water tank with no foam), and then the correct wave velocities can be back calculated.

2.3. Artificial aluminium properties. There is the need to create two experiment setups. On one hand, the aluminium Young's modulus and density is multiplied by a factor

$\beta = 10$ (point A in figure 2.2). This increases the impedance contrast between the two phases high enough that the effective wave velocity measured is only influenced by the parameters of the water phase (no coupling between aluminium and water phase). Indeed, it was observed from the simulation that no wave was traveling through the aluminium phase.

From the assumption above, using the high-frequency limit of Biot's equations, the turtuosity can be calculated for the geometry of this foam (since turtuosity is the only unknown). The measured effective wave velocity is $v_{p,fast}$=1409 m/s. This velocity is much lower as the reference velocity of homogeneous water $v_{p,water}$=1480 m/s. The result from Biot's equation for the tortuosity parameter is α_∞=1.14.

2.4. Real aluminium properties. Using the real physical aluminium properties in the simulation, there is an effective wave velocity $v_{p,fast}$=1487 m/s. On figure 2.1 a snapshot in one of the timesteps shows the wave traveling though both phases and through the aluminium phase alone. It can be observed that there is a coherent wave propagating through the water and aluminium phase. On the other hand, there is no coherent (or measureable) wave passing through the aluminium phase by itself.

3. Conclusion

In figure 2.2, v_p is calculated analytically from Biot's equations for different stiffening values β. If the isoline α_∞=1.14 is plotted over the parametric surface, the value B will be equivalent to calculating the fast P-wave velocity of the water saturated foam with real aluminium properties. Therefore if we compare the values of the numerical simulation and the analytical solution the measure how fit is the method. It was found that the analytical and the numerical solution match exactly. This methodology has proven to be highly effective for the computation of geometric properties such as tortuosity. Our numerical laboratory is not only limited to aluminium foams or homogeneous structures, which makes it a very robust and powerful tool.

Bibliography

[1] David B. Asay, Erik Hsiao, and Seong H. Kim. Effects of adsorbate coverage and capillary on nano-asperity friction in atmosphere containing organic vapor. *Journal of Applied Physics*, 110(6):064326, 2011.

[2] Wen-Yea Jang, Andrew M. Kraynik, and Stelios Kyriakides. On the microstructure of open-cell foams and its effect on elastic properties. *International Journal of Solids and Structures*, 45(78):1845 – 1875, 2008.

[3] Holger Steeb. Ultrasound propagation in cancellous bone. *Archive of Applied Mechanics*, 80(5):489–502, 2010.

[4] Erik H. Saenger, Norbert Gold, and Serge A. Shapiro. Modeling the propagation of elastic waves using a modified finite-difference grid. *Wave Motion*, 31(1):77 – 92, 2000.

CHAPTER 3

Numerical Analysis of Wave Propagation in Fluid-filled Deformable Tubes

The evaluation of new theories of wave propagation in porous media is discussed in this paper. As a result, the modern theory of Bernabe on wave propagation was found to be more suitable in Biot's low frequency domain. This paper was presented on the 84th Annual Meeting of the International Association of Applied Mathematics and Mechanics in Novi Sad, Serbia, March 18-22, 2013

- David Uribe[1,2]
- Holger Steeb[1]
- Erik H. Saenger[3]
- Patrick Kurzeja[2]
- Oscar E. Ruiz[1]

[1] CAD CAM CAE laboratory, Universidad EAFIT
Carrera 49 No 7 Sur - 50, Medellin, Colombia
[2] Mechanics – Continuum Mechanics, Ruhr-University
Bochum, Germany
[3] Geological Institute, ETH
Zuerich, Switzerland

Abstract. The study of wave propagation in fluid saturated deformable tubes is of great interest in biological and geological applications. It is also a simplified model of a porous material, and therefore the physical findings of such model can be extended into more complex models. The solution proposed by Biot neglected the mechanical interaction between the fluid and the solid phases at the microscopic level, and based his . In contrast, a more modern approach by Bernabe does take into account the deformation of the solid at a microscopic level. Using a Finite Difference code, the wave propagation phenomena was simulated. The wave source was modified with different characteristic frequencies in order to gain the information of the dispersion relation. It was found that the p-wave velocities of the simulations at sub-critical frequencies closely matches those of Bernabe's solution, but at over-critical frequencies they come closer to Biot's solution.

1. Introduction

In Biot's theory [1, 2], a wave propagating through a porous medium has different behaviors at two frequency domains. The first one is known as the low frequency domain, in which the wave propagating through the fluid phase is viscous dominated and has the form of poseuille flow. On the other hand, the high frequency domain allows the displacement field in the contact surface between the solid phase and the fluid phase to be decoupled. As a consequence, it is possible to find two p-wave modes from his equations. Furthermore, the wave traveling through the fluid phase has the form of plug flow.

Bernabe's solution [3] of the differential equations also have two characteristic frequency domains. The range of these domains match those found in Biot's theory. There are two great differences between Bernabe's and Biot's solutions. First, Bernabe uses only material properties based in the microscale, and Biot uses material properties related to the macroscale. The second difference is in the assumptions of the fluid deformation in the surface between the fluid and the solid phases. Biot restricts the deformation of the fluid phase only in volumetric change, but Bernabe assumes that the shearing deformation in this point may be different from zero.

The dispersion relation is the relationship between the wave speeds of a propagating wave against its frequency . It is possible to compare numerical, analytical and experimental results by comparing the dispersion relation of each approach.

2. Methodology

2.1. Analytical solutions. From the simplification given by Steeb (cf. [4]), eq. (8) shows the characteristic polynomial, with solutions $\xi_{1,2}$. From the relation $k_{1,2}^2 = \xi_{1,2}$, it is possible to find the wave number k. Then the p-wave velocities can be determined by the relation $c = \sqrt{k^2/w^2}$. The values of the parameters N, A, Q, R, P are effective material parameters that are calculated using Gedankenexperiment.

In Bernabe's solution, the characteristic polynomial is given by eq. (9). The terms: $J_i()$ is the Bessel function of the first kind, c_0 is the wave speed in the fluid phase, V_s is the wave speed in the solid phase, ρ is the fluid phase density and ρ_s is the solid phase density. The characteristic polynomial has four possible roots, but only two of them have a physical meaning.

$$0 = [PR - Q^2]\xi^2 - [P\hat{\rho}_{22} + R\hat{\rho}_{11} - 2Q\hat{\rho}_{12}]\xi + [\hat{\rho}_{11}\hat{\rho}_{22} - \hat{\rho}_{12}\hat{\rho}_{12}], \tag{8}$$

$$0 = c^4 - c^2\left(\frac{2J_1(kr)}{krJ_0(kr)}\frac{\rho}{\rho_s}c_0^2 + c_0^2 + 2V_s^2\right) + 2V_s^2c_0^2\left(1 - \frac{2J_1(kr)}{krJ_0(kr)}\right) \tag{9}$$

2.2. Numerical approximation. The geometry of the elastic tube is discretized using a regular three dimentional grid. The axial coordinate of the tube is oriented in the z-axis. The length of the elastic tube is not constant, since the wavelength of the induced wave in the elastic tube variates with its characteristic frequency. Therefore to avoid time consuming calculations, the length of the tube is changed to aproximately 2 wavelengths . The inner radius is $r = 0.25mm$ and the tube thickness is $h = 0.45$. The material properties of the solid phase is $V_p = 5330m/s$, $V_s = 3145m/s$, $\rho_s = 7900kg/m^3$ (similar to those of steel). The properties of the fluid phase is $c_0 = 1920m/s$, $\rho = 1258kg/m^3$ and $\eta = 1412cP$ (glycerol under standard conditions).

The elastodynamic wave equation can be extended by the anelastic functions as in eq. (10). These equations are solved using the finite difference method. In order to implement the viscoelastic properties of the fluid phase, the approach described in [5] is used to give the values to the anelastic coefficient tesor $\tilde{Y}_m^{ijkl}$. Other approximations of the anelastic coefficient tensor can be seen in [6, 7]. The time domain is discretized using a sencond order finite difference operator. The spatial derivatives are approximated by fourth order finite difference operators using a rottated staggered grid (RSG). The time and spatial discretization are solved explicitely in the the code.

The elastic tube is loaded at one end of the tube with a planar wave perpendicular to the z-axis. The induced wave is a first derivative of a normal distrubution with a characteristic frequency f_c.

$$\sigma_{ij} = C_{ijkl}\varepsilon_{kl} - \sum_m^{ij} \xi_m^{ij}, \qquad \dot{\xi}_m^{ij} + \omega_m \xi_m^{ij} = \omega_m \tilde{Y}_m^{ijkl}\varepsilon_{kl}. \tag{10}$$

3. Results

The numerical simulation can be seen on fig. 3.1. The phase velocities can be calculated from the first arrivals of the waves between the first and last snapshot. From the disperion relation in fig. 3.2, it can be seen that at sub-critical frecuencies, the numerical results are closer to Bernabe's solution. At over-critical frequencies the numerical results resemble Biot's solution. It was observed that in the high frequency domain, the flow is indeed that of a plug flow.

4. Conclusions and Future work

The theories of wave propagation in porous media of Biot and Bernabe were compared with a numerical simulation using the finite difference method. The numerical results were compared with analytical solutions. Future work aims to compare the velocity profile of the fluid phase between the numerical simulations and the analytical solutins, simulation of 2 and 3 dimentional lattices and the simulation of viscous solid materials.

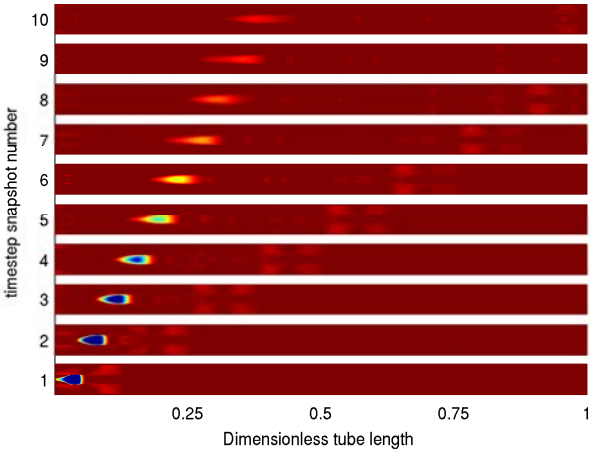

FIGURE 3.1. Cross sectional view of the propagating wave in the middle plane along the axial direction. f_c =150KHz. Colormap range optimal to visualize the slow p-wave. Wave progagation direction is left to right.

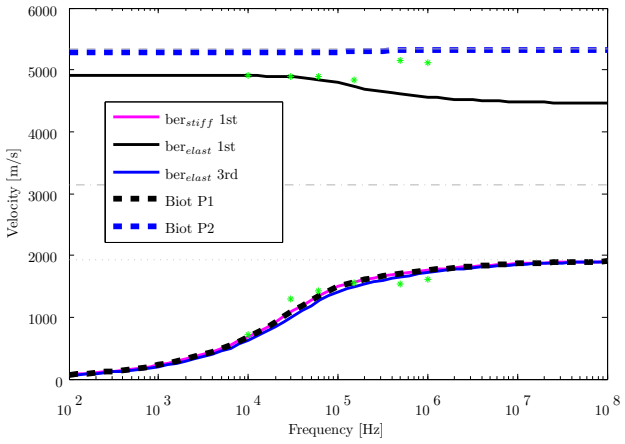

FIGURE 3.2. Disperion relation for the theories of Biot and Bernabe together with the numerical results. The green stars are the measured phase velocities from the simulations.

Bibliography

[1] M. A. Biot. Theory of propagation of elastic waves in a fluid-saturated porous solid. i. low-frequency range. *The Journal of the Acoustical Society of America*, 28(2):168–178, 1956.

[2] M. A. Biot. Theory of propagation of elastic waves in a fluid-saturated porous solid. ii. higher frequency range. *The Journal of the Acoustical Society of America*, 28(2):179–191, 1956.

[3] Rosolino Cirrincione, Eugenio Fazio, Patrizia Fiannacca, Gaetano Ortolano, and Rosalda Punturo. Microstructural investigation of naturally deformed leucogneiss from an alpine shear zone (southern calabria-italy). In Sergio Vinciguerra and Yves Bernab, editors, *Rock Physics and Natural Hazards*, Pageoph Topical Volumes, pages 995–1010. Birkhuser Basel, 2009.

[4] Holger Steeb. Ultrasound propagation in cancellous bone. *Archive of Applied Mechanics*, 80(5):489–502, 2010.

[5] E. H. Saenger, S. A. Shapiro, and Y. Keehm. Seismic effects of viscous biot-coupling: Finite difference simulations on micro-scale. *Geophysical Research Letters*, 32(14):n/a–n/a, 2005.

[6] Peter Moczo, Jozef Kristek, and Peter Franek. Lecture notes on rheological models. 2006.

[7] J. M. Carcione. Wave propagation in anisotropic linear viscoelastic media: theory and simulated wavefields. *Geophysical Journal International*, 101(3):739–750, 1990.

CHAPTER 4

Estimation of Large Domain Al Foam Permeability by Finite Difference Method.

It is of great interest to develop numerical methods to calculate the permeability value of fluid saturated porous media. The results of this research is the creation of a numerical method to estimate the permeability of porous media using CT-Scan large data. This paper was possible due to the collaboration between the CAD/CAM/CAE Laboratory at Universidad EAFIT and the Chair of Continuum Mechanics at Ruhr-Universitaet Bochum. It was presented on the 84th Annual Meeting of the International Association of Applied Mathematics and Mechanics in Novi Sad, Serbia, March 18-22, 2013.

- Maria Osorno[2]
- David Uribe[1,2]
- Oscar E. Ruiz[1]
- Holger Steeb[2]

[1] CAD CAM CAE laboratory, Universidad EAFIT
Carrera 49 No 7 Sur - 50, Medellin, Colombia
[2] Institute of Mechanics, Ruhr-University
Bochum, Germany

Abstract. The classical methods to calculate permeability of porous media have been proposed mainly for high density (e.g. granular) materials. These methods present shortcomings in high porosity media (e.g. metallic foams). While for dense materials permeability seems to be a function of the bulk properties and occupancy averaged over the volume, for highly porous materials these parameters fail to predict it. Several authors have attacked the problem by solving the Navier-Stokes equations for the pressure and velocity of a liquid flowing through a small domain (Ω_s) of aluminium foam and by comparing them with experimental values (prediction error approx. 9%). In this article we present calculations for much larger domains (Ω_L) using the Finite Difference (FD) method, solving also for the pressure and velocity of a viscous liquid flowing through the *Packed Spheres* scenario. The ratio $Vol(\Omega_L)/Vol(\Omega_s)$ is around 10^3. The comparison of our results with the Packed Spheres example yields a prediction error of 5% for the permeability. We also solved for pressure and velocity in an accurately modelled porous medium. Our geometric modelling of the porous domain stems from 3D X-ray tomography, yielding voxel information, which is particularly appropriate for FD. Ongoing work concerns the reduction in computing times of the FD method, consideration of other materials and fluids, and the enlarging of experimental work.

1. Introduction

Permeability is an important property in the design of filters of metallic foam, porous implants and other applications that require a flow through a porous medium ([1]). In this article we estimate the permeability of high porosity Aluminium foam ($\epsilon > 0.8$) employing the Finite Difference method . For the numerical estimation of the permeability for metallic foams the following methods have been used: (1) Finite Volumes, (2) Lattice Boltzmann, (3) Finite Difference Method. Gerbaux et al. ([2]) calculate the permeability of 3 real metallic foams by solving the Stokes equation in the porous medium with the Lattice Boltzmann method and the finite volume method. Xu et al. ([3]) perform a finite volume analysis to estimate the permeability of some foams cells with different porosities and porous diameter.
Petrasch et al. ([4]) determine porous media properties such as porosity and permeability from a digital representation of reticulate porous ceramics generated by X-ray tomographic scans. Nabovati et al. ([5]) calculate the permeability for fibrous porous media in a wide range of porosity by applying Darcy's law.
At present, only small domains of high porosity metallic foams are addressed for numerical estimation of permeability, given the computing expenses involved. In response to such limitations we implement FD, that is highly compatible with 3D Computer Tomography

2. Methodology

We propose a straightforward method to estimate the permeability of porous media: (1) Discretization of equations 11 and 13 on a staggered grid by using a 2nd order FD method with periodic boundary conditions for velocity in the inlet and outlet of the channel (Fig. 4.1). (2) Solution of the resulting equation system (Eq. 16, 17, 18, 19) with the method Gauss-Seidel iterative. This method does not require the storage of a coefficient matrix, therefore allowing to simulate larger domains. (3) Calculation of the volume average velocity u_m from the velocity field computed in step 2. (4) Estimation of the medium permeability with Darcy's law (Eqs. 15). The notation used is: K_D = Porous medium permeability according to Darcy's law, μ = Fluid dynamic viscosity, u_m = Volume average velocity of the fluid in the free volume, ΔP = Pressure drop in the flow direction.

$$\nabla p = \mu \nabla^2 \mathbf{u} \quad (11) \qquad \nabla \cdot \mathbf{u} = 0 \quad (12) \qquad \nabla \cdot \nabla p = 0 \quad (13)$$

$$u_m = \frac{\int_{V_f} |\mathbf{u}| dV}{V_f} \quad (14) \qquad K_D = \frac{\mu L u_m}{\Delta p} \quad (15)$$

$$p_{xx} + p_{yy} + p_{zz} = 0 \quad (16) \qquad p_x = \mu(u_{xx} + u_{yy} + u_{zz}) \quad (17)$$

$$p_y = \mu(v_{xx} + v_{yy} + v_{zz}) \quad (18) \qquad p_z = \mu(w_{xx} + w_{yy} + w_{zz}) \quad (19)$$

2.1. Method Validation. The method was validated with a regular packed sphere case in 3D (Fig. 4.2) whose permeability can be calculated with the Carman-Kozeny model proposed in [6] (Eq. 20) and with the Rumpf and Gupte model proposed in [7] (Eq. 21). The notation used is: K_C = Permeability by Carman-Kozeny model, K_R = Permeability by Rumpf and Gupte model, d = Sphere diameter and ϵ = Medium porosity (Volume free / Volume total). The relative error between the estimated permeability for a regular pack of spheres in a channel with 10 spheres in direction Z ($Sph_z = 10$) and the Rumpf and Gupte model was 5.5% .

$$K_C = \frac{\epsilon^3}{180(1-\epsilon)^2} d^2 \quad (20) \qquad K_R = \frac{\epsilon^{5.5}}{5.6} d^2 \quad (21)$$

3. Results

The permeability of an aluminium foam was estimated for a domain of $24mm \times 24mm \times 24mm$ ($400 \times 400 \times 400$ voxels). Figure 4.3 shows the velocity in Z direction on plane YZ at x= $12mm$. The calculated results for this case are $u_m = 6.5093 * 10^{-9}\, m/s$ and $K_D = 7.7967 * 10^{-7}\, m^2$. Our implementation allowed the computation of $256 * 10^6$ degrees of freedom in a single processor.

4. Conclusions and Future work

The permeability of a lattice of aluminium foam was calculated with the Darcy's law, using Finite Difference method to simulate a viscous flow through the porous medium. The proposed method optimizes memory usage, therefore allowing to simulate large domains in single processors. Future work includes the reduction in the computing time, the modification of flow parameters such as the input flux and the estimation of the permeability of materials with different porosities.

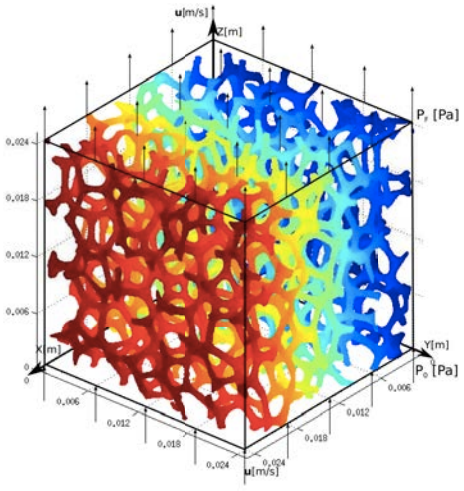

FIGURE 4.1. Domain $400 \times 400 \times 400$ voxels $(24mm \times 24mm \times 24mm)$.

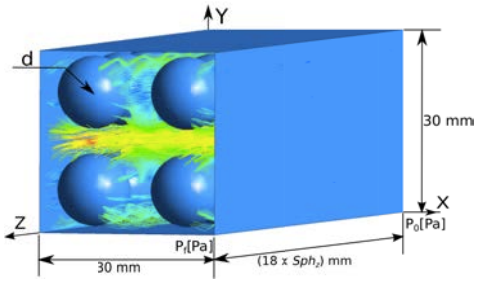

FIGURE 4.2. Regular packed sphere case

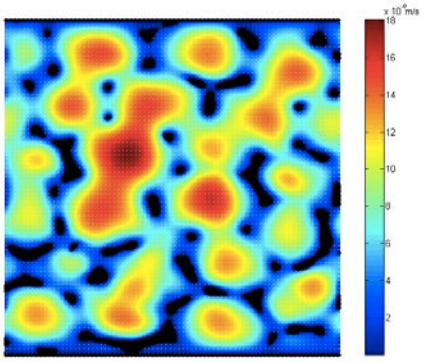

FIGURE 4.3. Velocity in Z direction on plane YZ at x= 12mm.

Bibliography

[1] L.P. Lefebvre, J. Banhart, D. Dunand, et al. Porous metals and metallic foams: current status and recent developments. *Advanced Engineering Materials*, 10(9):775–787, 2008.

[2] O. Gerbaux, F. Buyens, VV Mourzenko, A. Memponteil, A. Vabre, J.F. Thovert, and PM Adler. Transport properties of real metallic foams. *Journal of colloid and interface science*, 342(1):155–165, 2010.

[3] W. Xu, H. Zhang, Z. Yang, and J. Zhang. Numerical investigation on the flow characteristics and permeability of three-dimensional reticulated foam materials. *Chemical Engineering Journal*, 140(1):562–569, 2008.

[4] J. Petrasch, F. Meier, H. Friess, and A. Steinfeld. Tomography based determination of permeability, dupuit-forchheimer coefficient, and interfacial heat transfer coefficient in reticulate porous ceramics. *International Journal of Heat and Fluid Flow*, 29(1):315–326, 2008.

[5] A. Nabovati, E.W. Llewellin, and A. Sousa. A general model for the permeability of fibrous porous media based on fluid flow simulations using the lattice boltzmann method. *Composites Part A: Applied Science and Manufacturing*, 40(6):860–869, 2009.

[6] P.C. Carman. *Flow of gases through porous media*. Academic Press, 1956.

[7] HCH Rumpf and AR Gupte. Einflüsse der porosität und korngrößenverteilung im widerstandsgesetz der porenströmung. *Chemie Ingenieur Technik*, 43(6):367–375, 2004.

CHAPTER 5

Digital Material Laboratory: Wave Propagation Effects in Open-cell Aluminium Foams

The research in this paper compares the numerical, analytical and experimental calculation of effective material parameters of porous media. As a result, the image-based numerical approach was made into an effective tool for geophysical applications. This paper is the result of a multidisciplinary research endeavor between the CAD/CAM/CAE Laboratory at Universidad EAFIT, the Chair of Continuum Mechanics at Ruhr-Universitaet Bochum and the Geological Institute at ETH Zuerich. It was published in the International Journal of Engineering Science, Volume 58, September 2012, Pages 115-123; Publisher: Elsevier.
This publication is in the A1 category of the PUBLINDEX journal indexing system.

- E.H. Saenger[3]
- D. Uribe[1,2]
- R. Jaenicke[2]
- O. Ruiz[1]
- H. Steeb[2]

[1] CAD CAM CAE laboratory, Universidad EAFIT
Carrera 49 No 7 Sur - 50, Medellin, Colombia

[2] Mechanics – Continuum Mechanics, Ruhr-University
Bochum, Germany
[3] Geological Institute, ETH
Zuerich, Switzerland

Abstract. This paper is concerned with numerical wave propagation effects in highly porous media using digitized images of aluminum foam. Starting point is a virtual material laboratory approach. The Aluminum foam microstructure is imaged by 3D X-ray tomography. Effective velocities for the fluid-saturated media are derived by dynamic wave propagation simulations. We apply a displacement-stress rotated staggered finite-difference grid technique to solve the elastodynamic wave equation. The used setup is similar to laboratory ultrasound measurements and the computed results are in agreement with our experimental data. Theoretical investigations allow to quantify the influence of the interaction of foam and fluid during wave propagation. Together with simulations using an artificial dense foam we are able to determine the tortuosity of aluminum foam.

1. Introduction

Digital material methodology combines modern microscopic imaging with advanced numerical simulations of the physical properties of materials. One goal is to complement physical laboratory investigations for a deeper understanding of relevant physical processes. Large-scale numerical modeling of elastic wave propagation directly from the microstructure of the porous material is integral to this technology.

In this paper, we numerically consider a highly porous, open-cell aluminium foam. This special material is suitable for various applications in mechanics and engineering, e. g. as light-weight construction elements, mechanical filters or chemical catalysers. Besides its own applicability, open-cell aluminium foam has certain mechanical properties (porosity, intrinsic permeability, tortuosity etc.) which are similar to various cellular materials such as trabecular bone or polyurethane foam. Thus, various results of the present investigation can be transformed directly e. g. to the non-invasive diagnostics of cancellous bone.

Open-cell aluminium foam can be fabricated using open-cell polymer foam as template structure which is replaced by aluminium during a casting process. The resulting aluminium skeleton is built up as an irregular polyhedral network accounting for high porosity and effective hydraulic permeability, cf. Figure 5.1.

In order to investigate the complex wave propagation phenomena in this material, we split the considerations in three parts. First, we explain our applied digital material workflow. The specific workflow is put into context with other known approaches. Second, we discuss and present a specific numerical setup to investigate highly porous media using finite-difference wave simulations on a microscale. This section will be complemented by a description on aspects of numerical accuracy. Third, we present and evaluate the results for aluminium foam. These numerical results, which contain the physical processes on the pore scale, allow us to understand observations on a much larger scale (i.e., the sample scale).

2. Characterization of the material

For the present study, we analyze a 10 ppi AlSi7Mg foam (m.pore GmbH, Dresden, Germany). For quasi-static loading conditions, this material exhibits a linear-elastic range followed by a pronounced plateau stress in the stress-strain relation [1, 2]. Already for moderate compressive stresses, single layers of the skeleton start to fail which leads to

a subsequent collapse of the entire structure. However, this paper will focus on sound and ultrasound propagation effects with small amplitudes and we restrict ourselves on purely elastic material properties. The bulk properties of aluminium forming the porous skeleton can be characterized with standard testing methods. The mechanical properties of the ligaments (Young's modulus, Poisson's ratio, density) are known from quasi-static experiments [3], cf. Table 5.1.

In Figure 5.2, a typical pore of the investigated foam is depicted. The morphological properties discussed in this section are derived from the depicted single cell, which we consider to be representative for all cells. Stochastical considerations are not included in this part of the paper. Due to gravity effects during the processing of the polymer template, an intrinsic anisotropy of the structure can be observed. The cells are elongated in z direction by the anisotropy factor $\tau = 1.25$. Note that, within this contribution, all mechanical and numerical experiments are carried out with respect to this elongated z direction. We measure the cell size to account 7.3 mm in z direction and 5.8 mm in x and y direction, respectively. Furthermore, we find a typical ligament length of 2.0 mm. In Figure 5.3, the cross sections of one ligament are depicted. Again, the depicted ligament is considered to be representative for all ligaments within the specimen without further stochastical considerations. One observes the ligament to take a bone shape with a cross section which varies from a nearly triangular shape close to the ligament nodes to a more and more circular shape with increasing distance from the nodes. At the central position we observe a cross section area of $A = 0.1912\,\mathrm{mm}^2$.

Altogether, we find the micromorphological properties to be close to the properties of the foam evaluated in [3]. However, the cross sectional areas of the ligaments given by Jang et al. ($A = 0.296\,\mathrm{mm}^2$) seem to be considerably larger than for the microstructure investigated in the present contribution. Thus, the effective material properties, in particular the effective Young's modulus of the skeleton, can also be expected to be considerably lower than that one found by [3].

Besides the material properties of the ligaments the effective properties of the skeleton are to be investigated in mechanical experiments. As data basis, a set of 3 aluminium foam samples (40 mm×40 mm×40 mm) has been investigated. The average porosity has been measured by weighing as $\phi = 0.933$. By uniaxial compression tests (Schenck-Trebel universe testing device, 1 kN load cell) in direction of elongated cells (z direction) within the linear-elastic (pre-buckling) regime have resulted in the Young's modulus of the frame $E = 55.21\,\mathrm{MPa}$ (standard deviation 5.30 MPa) and a bulk modulus of $K = 18.40\,\mathrm{MPa}$ (standard deviation 1.77 MPa). In the experiments, a Poisson effect could not be observed, i.e. we assume that Poisson's ratio equals zero ($\nu = 0$).

Let us compare our data first to the analytical estimations by [1], where Young's modulus of the frame is proposed to equal

$$E = C_1\, E^s\, (1-\phi)^2. \tag{22}$$

If the fitting parameter is, as usual in the related literature, assumed to $C_1 = 1$, Gibson and Ashby predict $E = 277.83\,\mathrm{MPa}$. By contrast, the experimental data by [3] determine $E = 595.47\,\mathrm{MPa}$, i. e. one order of magnitude larger than our measurement. However, we want to state that the results can not be expected to be identical. Whereas the analytic estimation by Gibson and Ashby assumes a simplified cell geometry, the measurements of Jang et al. are related to a skeleton with slightly different properties of the single cells. In particular the diameter of the ligament cross sections, which has been observed to be considerably larger in the frame investigated by Jang and al., influences considerably the effective properties for local bending dominated deformations during overall compression of the sample.

At that time, no further geometrical and hydro-mechanical properties such as the effective hydraulic permeability have been determined yet in physical experiments.

3. Digital material laboratory workflow

3D X-ray microtomographic imaging and subsequent numerical determination of effective material properties is nowadays applied by various groups [4, 5, 6, 7, 8], to name only a few. Tomographic imaging can be routinely performed over three orders of magnitude in length scale with correspondingly high data fidelity. This capability, coupled with the development of advanced computational algorithms for image interpretation, three-dimensional visualization, and structural characterization and computation of physical properties based on image data, allows for a numerical laboratory approach to study real heterogeneous materials [5].

Several processing steps are important for such a virtual material laboratory. It starts with a Computer Tomographic (CT) scan of a selected material sample. The phase segmentation, which can be complicated for strongly heterogeneous materials, is required to build an appropriate digital model [9]. This model can be used for flow simulations [10, 11, 12]. They can provide realistic distributions of multiple fluids (e.g., patterns of wetting and non-wetting fluids) and effective transport properties (e.g., permeability). With exactly the same digital rock structure effective mechanical properties can be defined [13, 14, 15]. This allows to consider relationships between transport and mechanical properties, both depending on the microscopical properties.

At this point, it is also possible to calibrate the numerical results with laboratory measurements determining macroscopical effective properties (or vice versa). While the numerically determined permeability values fit the experimental data relatively well, there is a mismatch for the mechanical properties in the case this technique is applied to low porous rocks [16, 17, 18]. A systematic numerical overestimation of elastic moduli is reported. A possible reason is the limited resolution of X-ray techniques; features below that limit seem to play an important role (e.g., physics of grain contacts and tiny unresolved voids or cracks). However, for the considered aluminium foam we do not expect such resolution issues. A next step is to go from static to dynamic wave propagation simulations [19]. Although the macroscopic theory of wave propagation in porous fluid-saturated media has been established 50 years ago [20] there are still many unresolved questions about the physical origin of attenuation, dispersion and high frequency wave propagation in such media.

We concentrate on the Rotated Staggered Grid (RSG) Finite-Difference (FD) method [21] for pore-scale simulation of wave propagation in digitized materials.

3.1. Digital aluminium Foam Sample. X-ray-based tomographic microscopy [22] is suitable to provide data on the real pore microstructure of materials. To demonstrate the proposed workflow we have selected the open-cell aluminium foam introduced earlier. However, other samples can be used as well. In Figure 5.5 we illustrate our final digitized model after several processing steps. These include discontinuity detection, thresholding and region processing [23]. The digital aluminium foam contains 2 different phases: solid aluminium phase (colored) and the porous space (transparent). For the numerical analysis, we use a 3D-image of the aluminium foam discretized on a regular cartesian grid with 400 $\times$ 400 $\times$ 400 grid points. The pores as well as the aluminium are 100 % connected besides some ligaments at the boundary.

3.2. Numerical Simulation of Wave Propagation in aluminium Foam. To study wave propagation effects in the digitized aluminium foam sample (Figure 5.4) numerically, we use a technique similar to the approach described in [24, 25]. The basic idea is to study speeds of elastic waves through heterogeneous materials in the long wavelength limit (pore size $\ll$ wavelength) using the RSG FD algorithm [21]. In the case of fluid-saturated highly porous media (porosity $\geq$ 80 %) it is necessary to modify the numerical setup compared to the case for low porosity materials (porosity $\leq$ 35 %). This is described below. A review of related methods is given in [14, 25].

For the purpose of studying wave propagation effects of aluminium foam the digitized material is embedded into a homogeneous region, Figure 5.5. In this study we assign to this region the elastic properties of non-viscous water. Related to a classical experimental setup, this is similar to through-transmission-experiments in an immersion technique. This is in contrast to a homogeneous elastic stiff rock embedding applied in [24]. With this modified embedding we reach a better coupling to the saturated aluminium foam and a longer wavelength can be numerically inserted.

The full synthetic models are made up of $804 \times 400 \times 400$ grid points. We perform our experiments with periodic boundary conditions in the directions parallel to the wave propagation process. A body force plane source at the top of the model is applied. A plane P-wave generated in this way propagates through the numerical model as shown in Figure 5.6. The broadband source in our experiments is always the first derivative of a Gaussian wavelet. The dominant frequency is given among other modeling parameters in Table 5.1. All computations are performed with second order spatial FD operators and with a second order time update. With two planes of receivers at the top and at the bottom of the model, it is possible to measure the time-delay of the peak amplitude of the mean plane wave caused by the inhomogeneous structure of the digitized material sample. With the time-delay (compared to a reference model) one can estimate the effective velocity of compressional waves [24]. In general, two different kinds of P-waves can be expected for porous media. Fist a fast compressional wave and second a so-called slow (Biot) wave, cf. [20, 26].

Next, we analyze 2 distinct cases of fluid-saturated aluminium foam numerically. At first, we compute aluminium foam which is saturated with a (non-viscous) fluid. In the second case, we modify the properties of aluminium (Young's/compression modulus, density: factor 10 higher, each). Assuming Poiseuille flow we can calculate the viscous skin depth as a function of frequency ω [27, 28]

$$d = \sqrt{\frac{2\,\eta^{fR}}{\omega\,\rho^{fR}}}, \tag{23}$$

where ρ^{fR} denotes the effective (true) density of the fluid and η^{fR} the effective dynamic fluid viscosity.

If the pore radius r is larger than the viscous skin depth d we investigate the high-frequency domain which is characterized by an additional inertia coupling mechanism between the solid and the fluid phase. As in our microstructure-based analysis the pore radius r is known, we are able to calculate this critical frequency (transission frequency)

$$f^{crit} = \frac{\eta^{fR}}{\rho^{fR}\,\pi\,r^2} < 1\,\text{Hz}. \tag{24}$$

Even if we assume Johnson and Plona's formula to estimate a travelling second wave, known as the viscous frequency,

$$f^{visous} = \frac{\eta^{fR}}{\rho^{fR}\,\pi\,r^2\,\xi},\ \xi \approx 0.01, \tag{25}$$

we expect to end up in the high-frequency range above 100 Hz.

3.3. Case 1: Water-saturated Aluminuim Foam. From a theoretical point of view we consider here the high frequency range of Biot's velocity relations because we saturate our digitized image of aluminium foam with a non-viscous fluid (effective dynamic fluid viscosity $\eta^{fR} = 0$). In the case of highly porous media, the most dominant wave is that one which is travelling mainly through the fluid phase. The effective velocity is $v_{p,fast} = 1487$ m/s. This is slightly faster compared to the case of homogeneous water ($v_{p,water} = 1480$ m/s). A coherent P-wave travelling through the aluminim skeleton can not be detected clearly. Only some incoherent low-amplitude wave arrivals are visible.

Similar results are obtained in ultrasound through-transmission laboratory experiments. At room temperature ($\Theta \approx 20^\circ C$), we obtain a wave velocity in the water phase of $v_{p,water} = 1498$ m/s. If we perform an ultrasound experiment with the water-saturated aluminium foam sample, we observe a slightly faster P-wave of $v_{p,fast} = 1512$ m/s.

The numerical and experimental investigations can be compared to the high-frequency limits of Biot's equations [20, 26]. In Figure 5.7 we show the solution of the wave velocity for the fast wave of Case 1. If the tortuosity is small, i.e. if $\alpha_\infty \approx 1$, the wave velocity is slightly larger $v_{p,fast} = 1507$ m/s than the P-wave travelling through water ($v_{p,water} = 1483$ m/s). For larger values of tortuosity, the wave velocity becomes smaller. Note that we obtain a wave speed $v_{p,fast} = 1487\,\mathrm{m/s}$ in case of $\alpha_\infty = 1.14$.

3.4. Case 2: Water-saturated Artifical Stiff aluminium Foam. For this case, we assign to the aluminium foam stiffness and density parameters which are ten times higher then in Case 1. With this trick, from a numerical point of view very straightforward, we have an artifical stiff aluminium foam. With this simulation we want to understand if a signature of the elastic properties of the foam will influence the speed of the fast P-wave. Furthermore, we are able to examine the amount of tortuosity from this setup. From our numerical experiment we obtain in that case a fast P-wave velocity of $v_{p,fast} = 1409$ m/s. We therefore conclude that the measured wave speed for Case 1 is not a result of the fluid properties only. Comparing the numerical investigations with the high-frequency limits of Biot's equations, we are able to determine the turtuosity parameter of our aluminium foam. As turtuosity is the only physical effect which is responsible for a deviation of the fast P-wave from the wave travelling through homogeneous water, we obtain for the foam ($v_{p,fast} = 1409\,\mathrm{m/s}$) the turtuosity $\alpha_\infty = 1.14$.

Evaluating Biot's equation for Case 1 with $\alpha_\infty = 1.14$ predicts the theoretical P-wave velocity of water-saturated aluminium foam of $v_{p,fast} = 1487\,\mathrm{m/s}$ which is exactly the velocity we have observed in our numerical simulation.

4. Conclusions

In this paper we describe numerical, laboratory and theoretical estimations of effective acoustic properties of a highly porous media. The considered aluminum foam with a porosity of 0.923 is imaged by 3D X-ray tomography. With the known material properties of Aluminum and water we perform large-scale finite-difference wave propagation computations to estimate wave velocities of the fully saturated foam. Due to the high porosity we have to apply a specific numerical setup where the saturated sample is inserted in a homogeneous fluid environment. The laboratory and numerical measurements show excellent agreement. A detailed theoretical analysis, supported with simulations using artificial dense aluminum, gives three main results: First, our experiments took always place in the high-frequency limit of the Biot-theory. Second, the interaction between foam and fluid can not be neglected for estimating wave propagation effects. Third, we are able to determine the tortuosity of the aluminum foam to equal α_∞=1.14.

Used modeling parameters	
Young's modulus of aluminium	$E^s = 70.0$ GPa
Poisson number of aluminium	$\nu^s = 0.33$
Effective (true) density of aluminium	$\rho^{sR} = 2700$ kg/m^3
Bulk modulus of pore fluid	$K^f = 1.48$ GPa
Effective (true) density of pore fluid	$\rho^{fR} = 1000$ kg/m^3
Sample size (grid points)	$400 \times 400 \times 400$
Grid spacing	$\Delta h = 60.331$ μm
Sample thickness	$d = 400 \times 60.331$ μm $= 0.0241$ m
Porosity	$\phi = 0.923$ (from CT data)
Pore geometry	see Figure 5.2
Dominant frequency of used wavelet	$f_{dom} = 24$ kHz
Dominant wavelength@1480m/s	$\lambda_{dom} = 0.061$ m ≈ 2.6 d

TABLE 5.1. Modeling parameters and numerically estimated properties of the digitized aluminium sample shown in Figures 5.4, 5.5

Experimentally obtained data	
Porosity	$\phi = 0.933$
Effective Young's modulus (skeleton)	$E = 55.21 \pm 5.30$ MPa
Effective Poisson's ratio (skeleton)	$\nu = 0$
P-wave velocity (homogeneous water, $\Theta \approx 20°$)	$v_{p,water} = 1498$ m/s
P-wave velocity (water-saturated foam, $\Theta \approx 20°$)	$v_{p,fast} = 1512$ m/s

TABLE 5.2. Experimental data of the aluminium foam samples.

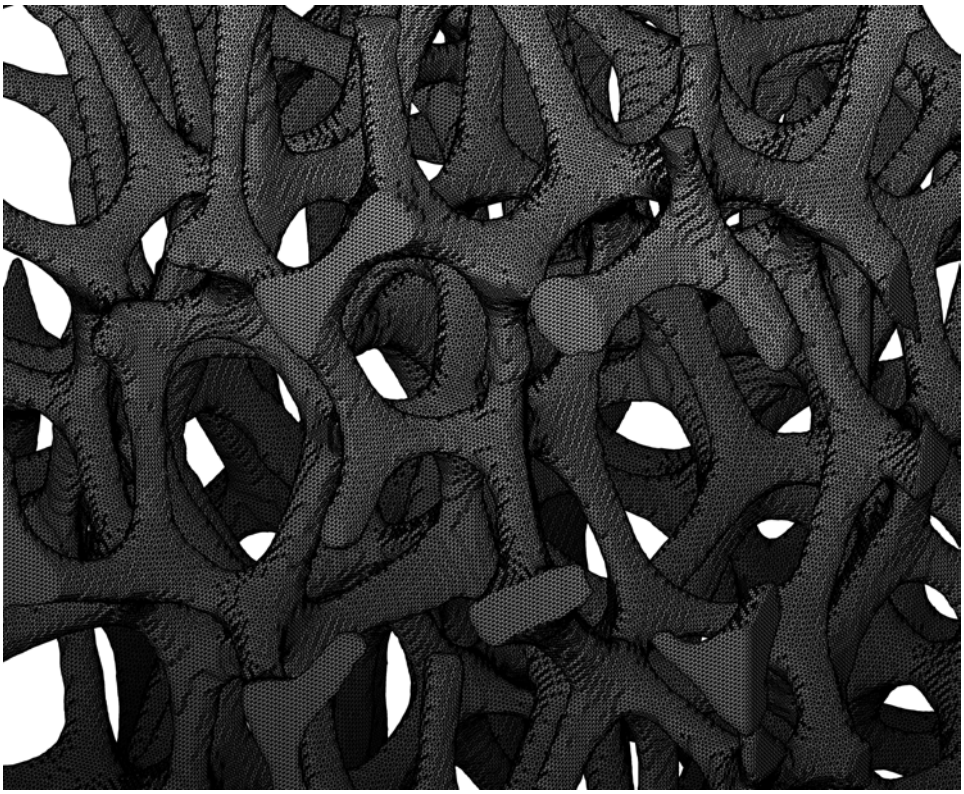

FIGURE 5.1. Irregular polyhedral network of the investigated open-cell aluminium foam. Detail from a CT reconstruction.

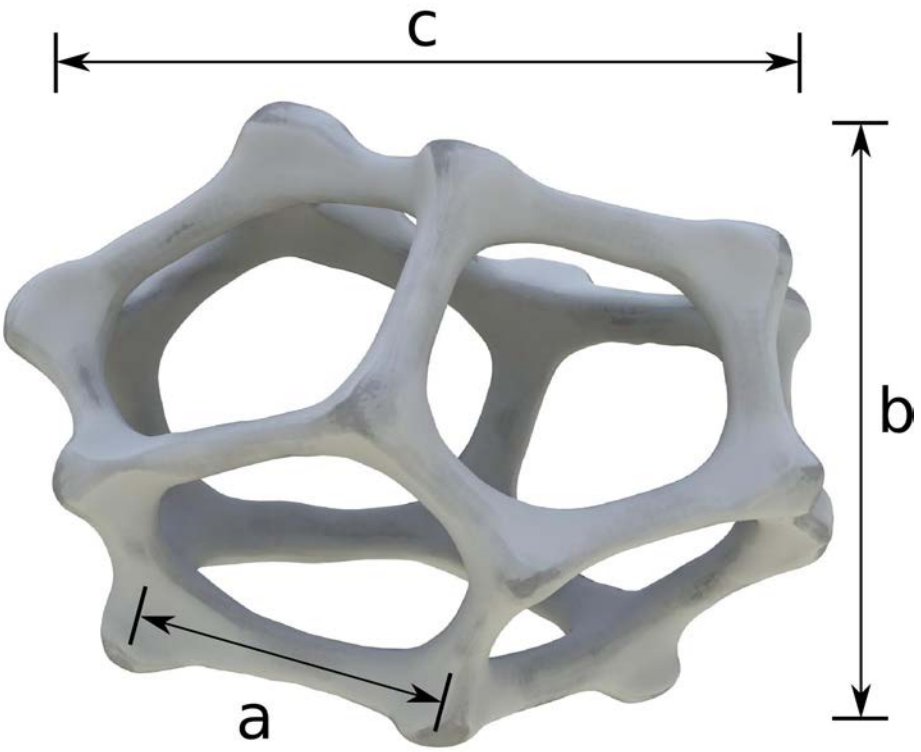

FIGURE 5.2. Exemplary cell of the aluminium foam with characteristic dimensions $a = 1.984\,\mathrm{mm}$, $b = 5.836\,\mathrm{mm}$, $c = 7.314\,\mathrm{mm}$ and anisotropy factor $\tau = c/b = 1.25$.

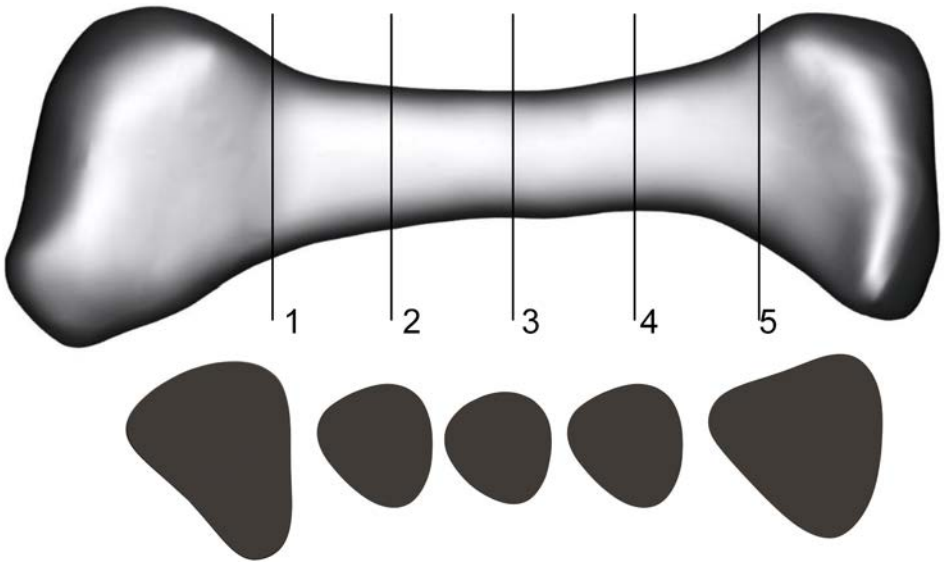

FIGURE 5.3. Single ligament of the aluminium foam with cross section areas $A_1 = 0.4616\,\mathrm{mm}^2$, $A_2 = 0.2081\,\mathrm{mm}^2$, $A_3 = 0.1913\,\mathrm{mm}^2$, $A_4 = 0.2289\,\mathrm{mm}^2$ and $A_5 = 0.4674\,\mathrm{mm}^2$. The cross section varies from a nearly triangular shape at the ligament nodes to a more circular shape in the ligament center.

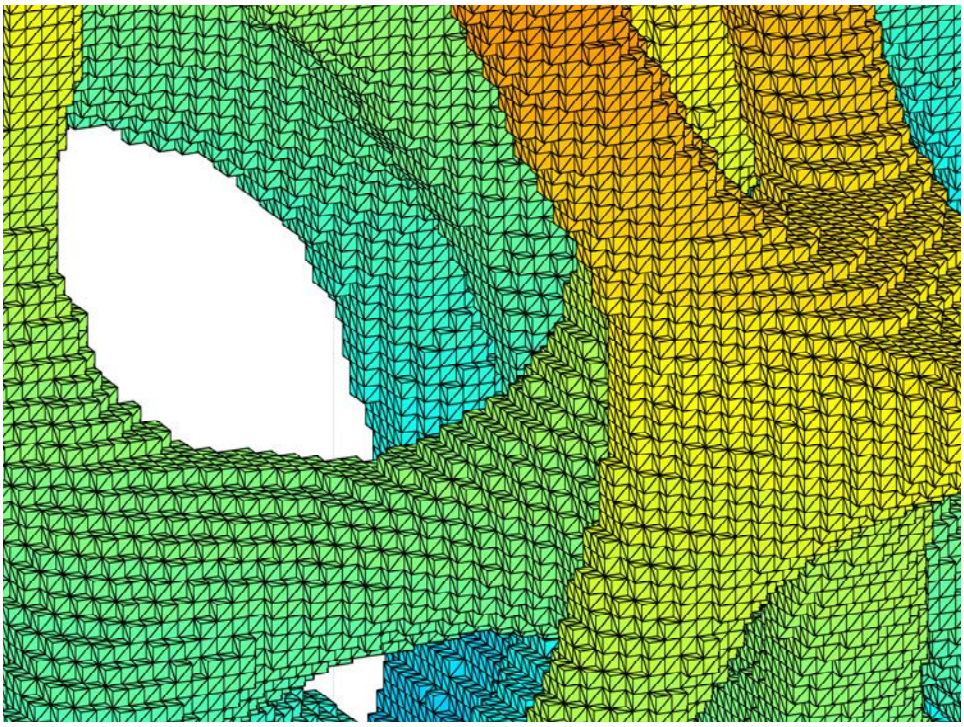

FIGURE 5.4. Boxel-based detail of the digitized aluminium foam model. The grid spacing accounts for $\Delta h = 60.331\,\mu$m.

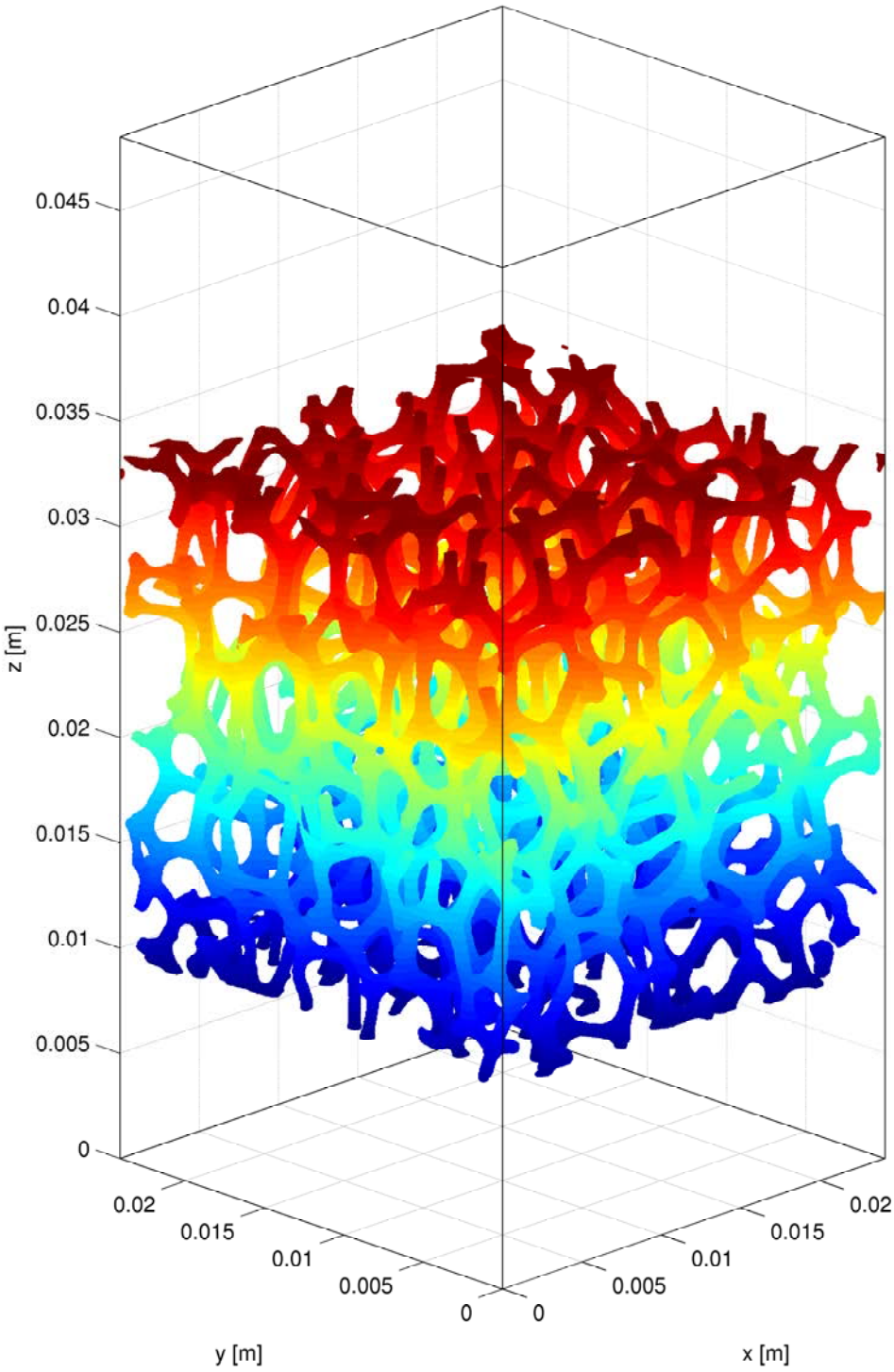

FIGURE 5.5. Investigated unit cell, aluminium (colored) and water (transparent).

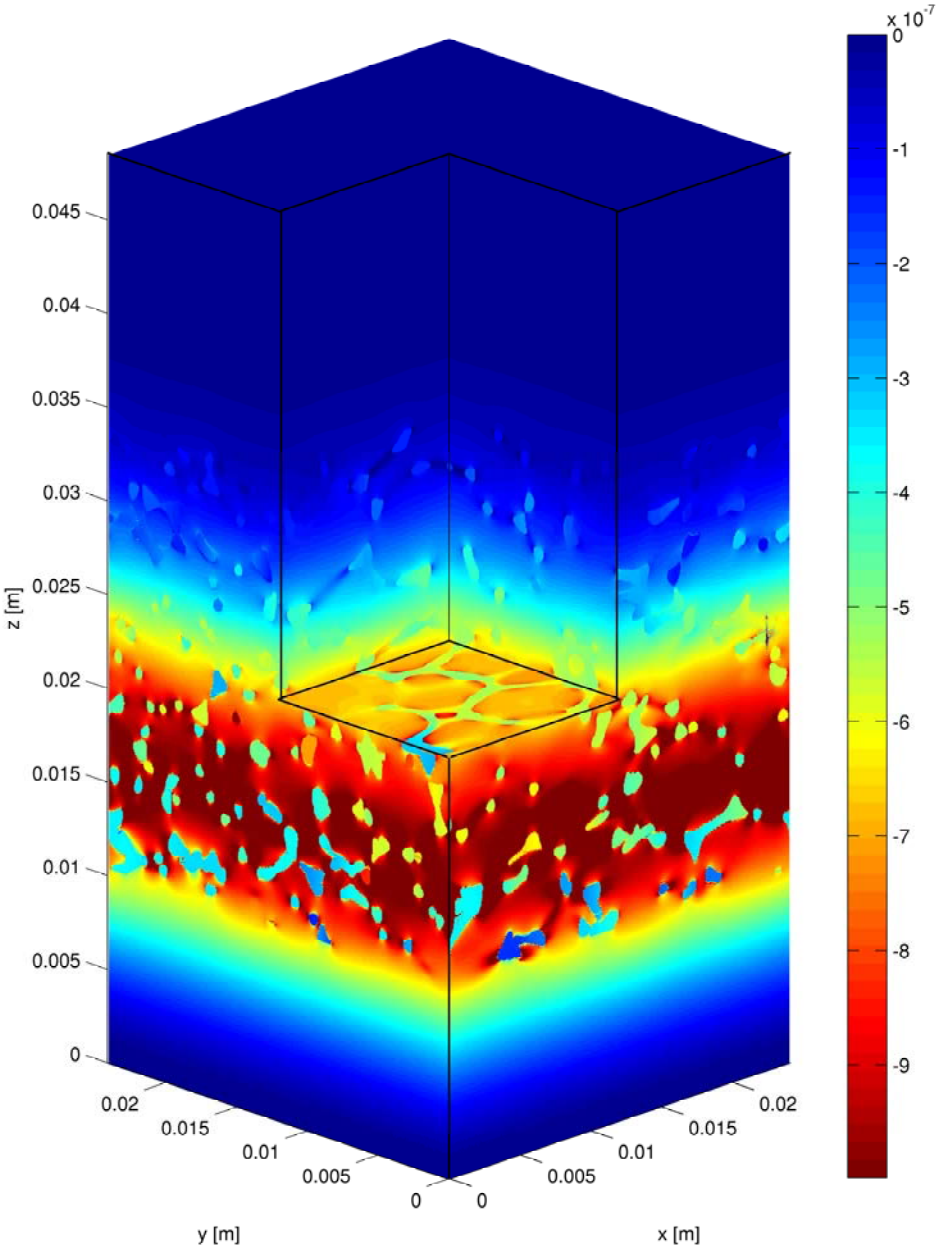

FIGURE 5.6. P-wave passing through the fluid-filled open-cell foam.

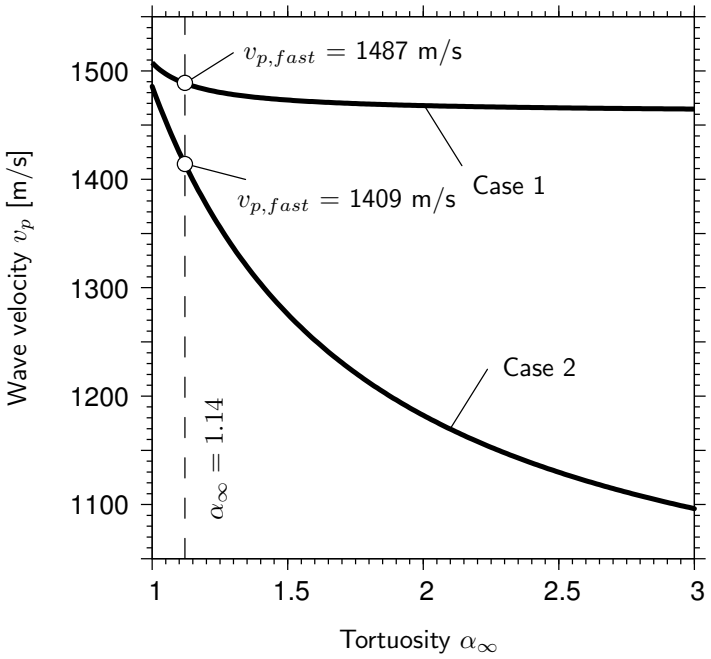

FIGURE 5.7. High-frequency solution of Biot's equations [26]. The phase velocity of the wave which mainly travels through the water phase is depicted for Case 1 and Case 2 depending on tortuosity.

Bibliography

[1] L. J. Gibson and M. F. Ashby. *Cellular solids. Structure and properties.* Cambridge Solid State Science Series. 1997.

[2] T. G. Nieh, K. Higashi, and J. Wadsworth. Effect of cell morphology on the compressive properties of open-cell aluminium foams. *Mat. Sci. Eng. A*, 283:105–110, 2000.

[3] W.-Y. Jang, A. M. Kraynik, and S. Kyriakides. On the microstructure of open-cell faoms and its effect on elastic properties. *Int. J. Solids Struct.*, 45:1845–1875, 2008.

[4] P.-E. Øren, S. Bakke, and R. Held. Direct pore-scale computation of material and transport properties for north sea reservoir rocks. *Water Resour. Res.*, 43:W12S04, 2007.

[5] A. Sakellariou, C. H. Arns, A. P. Sheppard, R. M. Sok, H. Averdunk, A. Limaye, A. C. Jones, T. J. Senden, and M. A. Knackstedt. Developing a virtual materials laboratory. *Mater. Today*, 10:44–51, 2007.

[6] I. Malinouskaya, V. V. Mourzenko, J.-F. Thovert, and P. M. Adler. Wave propagation through saturated porous media. *Phys. Rev. E*, 77:066302, 2008.

[7] J. Dvorkin, M. Armbruster, C. Baldwin, Q. Fiang, N. Derzhi, C. Gomez, B. Nur, and A. Nur. The future of rock physics: computational methods vs. lab testing. *First Break*, 26:63–68, 2008.

[8] E. H. Saenger. Time reverse charachterization of sources in heterogeneous media. *NDT & E International*, 44:751759, 2011.

[9] J.T. Fredrich, B. Menendez, and T.F. Wong. Imaging the pore structure of geomaterials. *Science*, 268(5208):276–279, 1995.

[10] C. H. Arns, M. A. Knackstedt, and W. V. Pinczewski. Accurate estimation of transport properties from microtomographic images. *Geophys. Res. Lett.*, 28:3361–3364, 2001.

[11] Y. Keehm, T. Mukerji, and A. Nur. Permeability prediction from thin sections: 3D reconstruction and lattice-boltzmann flow simulation. *Geophys. Res. Lett.*, 31:L04606, 2004.

[12] J. Harting, J. Chin, M. Venturoli, and P. V. Coveney. Large-scale lattice boltzmann simulations of complex fluids: advances through the advent of computational grids. *Philos. T. R. Soc. A*, 363:1895–1915, 2005.

[13] C. H. Arns, M. A. Knackstedt, W. V. Pinczewski, and E. J. Garboczi. Computation of linear elastic properties from microtomographic images: Methodology and agreement between theory and experiment. *Geophysics*, 67:1396–1405, 2002.

[14] E. H. Saenger. Numerical methods to determine effective elastic properties. pages 598–605, 2008.

[15] M. Madadi, A. C. Jones, C. H. Arns, and M. A. Knackstedt. 3D imaging and simulation of elastic properties of porous materials. *Comput. Sci. Eng.*, 11(4):65–73, 2009.

[16] M. A. Knackstedt, S. Latham, M. Madadi, A. Sheppard, T. Varslot, and C. H. Arns. Digital rock physics: 3D imaging of core material and correlations to acoustic and flow properties. *The Leading Edge*, 28(1):28–33, 2009.

[17] Y. Zhang. *Modeling of the effects of wave-induced fluid motion on seismic velocity and attenuation in porous rocks (Ph.D. thesis).* Massachusetts Institute of Technology, 2010.

[18] C. Madonna and E. H. Saenger. Digital rock physics: Calibration with laboratory measurements. *73nd EAGE Conference, Vienna, Austria*, 2011.

[19] E. H. Saenger, S. A. Shapiro, and Y. Keehm. Seismic effects of viscous Biot-coupling: Finite difference simulations on micro-scale. 32:L14310, 2005.

[20] M. A. Biot. Theory of propagation of elastic waves in a fluid-saturated porous solid I. Low-frequency range. 29:168–191, 1956.

[21] E. H. Saenger, N. Gold, and S. A. Shapiro. Modeling the propagation of elastic waves using a modified finite-difference grid. *Wave Motion*, 31(1):77–92, 2000.

[22] F. Marone, C. Hintermüller, S. McDonald, R. Abela, G. Mikuljan, A. Isenegger, and M. Stampanoni. X-ray Tomographic Microscopy at TOMCAT. *Journal of Physics: Conference Series*, 168:doi:10.1088/1742–6596/186/1/012042, 2009.

[23] R. C. Gonzales and R. E. Woods. *Digital Image Processing.* Prentice-Hall, 2002.

[24] E. H. Saenger, O. S. Krüger, and S. A. Shapiro. Effective elastic properties of randomly fractured soils: 3D numerical experiments. 52(3):183–195, 2004.

[25] E. H. Saenger, F. Enzmann, Y. Keehm, and H. Steeb. Digital rock physics: Effect of fluid viscosity on effective elastic properties. 74:236–241, 2011.

[26] G. Mavko, T. Mukerji, and J. Dvorkin. *The Rock Physics Handbook. Tools for seismic analysis in porous media.* 2003.

[27] E. R. Hughes, T. G. Leighton, G. W. Petley, P. R. White, and R. C. Chivers. Estimation of critical and viscous frequencies for biot theory in cancellous bone. *Ultrasonics*, 41:365–368, 2003.

[28] H. Steeb. Ultrasound propagation in cancellous bone. *Arch. Appl. Mech.*, 80:489–502, 2010.

Conclusions

From the present compilation it was possible to describe 3 techniques to characterize multi-phase materials at the microscale and therefore gain their effective properties at the macroscale.

The homogenization of micromechanical properties allows the use of advanced numerical methods like the FE^2. From the proposed homogenization approach, it is possible to upscale the micromechanical properties to the macroscale with the use of modified boundary conditions at the microscale level. This modification leads to the minimal loading conditions, which allows the use of micro volumina that are not necessarily periodic, and therefore it is possible to evaluate true heterogenous materials.

The use of finite diffence methods to simulate the wave propagation in multi-phase materials (e.g porous media) was used in two cases: (i) The numerical estimation of effective material parameters such as tortuosity, p-wave modulus and s-wave modulus and (ii) the benchmark of new theories of wave propagation in porous media.

It was shown that the finite difference approach closely matches the analytical results found in the literature. A new theory of wave propagation was evaluated and found to be accurate when compared to the numerical results given by the aforementioned method.

The finite difference method was also used for the solution of the stokes flow equation. From this approach, effective material parameters like the permeability were able to be caculated. The proposed method was tested against benchmark problems, and it was found to be consistent with analytical results. Furthermore, the permeability value of an aluminium foam was estimated.